Optimal Scheduling of Biogas-Solar-Wind Renewable Portfolio for Multi-Carrier Energy Supplies

Bin Zhou, *Senior Member*, *IEEE*, Da Xu, Canbing Li, *Senior Member*, *IEEE*, Chi Yung Chung, *Fellow*, *IEEE*, Yijia Cao, *Senior Member*, *IEEE*, Ka Wing Chan, *Member*, *IEEE*, Qiuwei Wu, *Senior Member*, *IEEE*

***Abstract*—This paper proposes a multi-source multi-product framework for coupled multi-carrier energy supplies with a biogas-solar-wind hybrid renewable system. In this framework, the biogas-solar-wind complementarities are fully exploited based on digesting thermodynamic effects for the synergetic interactions of electricity, gas and heating energy flows, and a coupling matrix is formulated for the modeling of production, conversion, storage, and consumption of different energy carriers. The multi-energy complementarity of biogas-solar-wind renewable portfolio can be utilized to facilitate the mitigation of renewable intermittency and the efficient utilization of batteries, and a multi-carrier generation scheduling scheme is further presented to dynamically optimize dispatch factors in the coupling matrix for energy-efficient conversion and storage, while different energy demands of end-users are satisfied. The proposed methodology has been fully tested and benchmarked on a stand-alone Microgrid over a 24-hour scheduling horizon. Comparative results demonstrate that the proposed scheme can lower the battery charging/discharging actions as well as the degradation cost, and also confirm its capability to accommodate high penetration of variable renewables.**

***Index Terms*—Energy hub, energy storage, renewable energy, Microgrid, multi-energy systems.**

I. Introduction

THE importance of hybrid renewable energy system (HRES) has been increasingly recognized for providing sustainable and reliable energy supply with low emissions and high fuel flexibility, especially for stand-alone power systems in remote areas [1]. The inherent intermittency and volatility of wind and solar power have raised concerns regarding the integration and utilization of high-penetration renewables in power systems [2], [3]. Energy storage system (ESS) is an effective technological solution for mitigating the fluctuations from renewable energy sources (RESs), and extensive efforts in [4]-[8] have been made to enhance the overall system availability of HRES with various ESSs. Among existing energy storage technologies, there is substantial interest in battery energy storage (BES) because of its efficient rechargeability, high energy density, and low maintenance advantages [5]. Nevertheless, the wear and tear caused by frequent charging and discharging would decrease battery cycle lifetime and storage capability, and thus the running cost of BES is expensive due to its short service life, which contributes significantly to the operating cost of HRES [2],[8]. This paper strives to cope with the effects of variable RESs through coupled multi-energy conversion from biomass energy sources so as to alleviate battery dependency.

Biogas is a promising renewable energy with significant potential to provide diversified energy services such as electricity, heating, and lighting [9],[10]. Biogas is commonly generated in anaerobic conditions from raw materials such as agricultural waste and dedicated energy crops. The produced biogas can be stored or converted into electricity and heat via a combined heat and power (CHP) plant, and then fed into power distribution system and local district heating network [11]. In addition, it can be further purified to pipeline-quality natural gas and injected in natural gas network [9]. Biogas energy is independent from climatic influences for offering high predictability and availability, and thus can be utilized to balance the stochastic energy production from weather-driven RESs [12]-[16]. The biogas integrated HRES can be formed as an energy hub to process multi-energy carriers including electricity, heat, and gas. Within the energy hub, different types of primary energy sources, such as biomass, solar and wind, can be converted and conditioned into desirable energy demands [17]. Consequently, this paper aims to investigate the hybrid renewable-based energy hub to manage the variability of RESs, and provide flexible multi-carrier energy services with optimal energy-efficient scheduling scheme.

The energy hub model was proposed in [18] to optimize the coupled power flows of multi-energy carriers, and further studies on the interconnected hubs, energy flow analysis, topological and structural designs of hub couplings were investigated in [19]-[24]. Furthermore, various renewable generations, such as wind, solar, and hydropower, have been integrated into energy hubs in [25]-[28] for economic and emission reductions, and the flexibility provided by mutual interconnections from multi-inputs to multi-outputs can be utilized to cope with the effects of variable RES penetration. Hybridization of multiple RES technologies in energy hubs can also improve system reliability and energy efficiency [29]-[31]. The biogas integrated HRESs were reported in [14],[16],[32]-[35] for combined heat and electricity generation, and the dependency on fossil fuels as well as environmental emissions can be alleviated. However, the coupling interactions between biogas and other RESs on multi-energy conversion and storage are not involved yet.

With the surge in fossil fuel prices and increasing environmental concerns, the 100% renewable energy systems are economically viable for providing investment opportunities due to

This work was jointly supported by the National Natural Science Foundation of China (51507056), Hunan Strategic Industries Scientific and Technological Project under Grant 2017GK4028, and the Hunan Natural Science Foundation of China (2017JJ3019).

B. Zhou, D. Xu, C. Li and Y. Cao are with the College of Electrical and Information Engineering, Hunan University, Changsha 410082, China, and also with the Hunan Key Laboratory of Intelligent Information Analysis and Integrated Optimization for Energy Internet, Hunan University, Changsha 410082, China (e-mail: binzhou@hnu.edu.cn; eedaxu@outlook.com; lcb@hnu.edu.cn; yjcao@hnu.edu.cn).

C. Y. Chung is with the Department of Electrical and Computer Engineering, University of Saskatchewan, Canada (e-mail: c.y.chung@usask.ca).

K. W. Chan is with the Department of Electrical Engineering, The Hong Kong Polytechnic University, Hong Kong (e-mail: eekwchan@polyu.edu.hk).

Q. Wu is with the Center for Electric Power and Energy, Department of Electrical Engineering, Technical University of Denmark, Kgs. Lyngby, 2800 Denmark (e-mail: qw@elektro.dtu.dk).

no fossil fuel requirement and low operating cost. The biogas-solar-wind HRES can provide a cost-competitive solution with higher complementarity and significance for stand-alone multiple energy supplies. In addition to the time complementarity between solar and wind resources [6], biogas plant can offset the diurnal fluctuations of intermittent RESs. Moreover, the available solar and wind generations can be utilized to heat the thermostatic digester in order to improve the efficiency of biogas production from anaerobic digestion [32],[33]. Hence, the biogas-solar-wind energy complementarities can be exploited based on digesting thermodynamic effects to accommodate the fluctuating RESs, and the excess wind and solar energy can be converted to biogas in a gas storage tank. The proposed biogas-solar-wind renewable portfolio can contribute towards the formation and development of stand-alone Microgrids for multi-energy supplies in the off-grid remote areas, such as rural villages and islands. As the performances of anaerobic organisms in the fermentation process are severely limited under cold digestion temperatures, the proposed HRES can also promote biogas applications in cold climates, and significantly decrease the cost of domestic waste treatment and pollution emissions as a result of biogas utilization instead of burning biomass sources.

In this paper, the biogas-solar-wind energy complementarities are proposed to form a coupled multi-carrier energy supply framework for stand-alone autonomous Microgrids. The contributions of this paper are summarized as follows: 1) A R-C thermodynamics-based thermal interaction model is formulated to investigate the digesting thermodynamic effects for harvesting fluctuating RESs in the form of biogas; 2) A biogas-solar-wind energy hub framework is proposed for mapping the input renewable energies to multi-energy demands, and a coupling matrix is formulated for the modeling of production, conversion, storage, and consumption of different energy carriers; 3) A rolling horizon based multi-carrier generation scheduling scheme is developed to optimize the multi-energy conversion pathways for system energy-efficiency enhancement.

II. Modelling of Biogas-Solar-Wind Energy Hub

A. Digesting Thermodynamic Analysis

Biogas can be produced from a wide range of organic wastes with anaerobic organisms, and its yield is determined by digestion temperature in a closed digester. For the mesophilic anaerobic digestion, temperature is an important environmental factor to control the rate and course of digestion [33]. In general, the increase in temperature of biogas digester leads to the rise in the substrate utilization rate and metabolic rate of digestion microorganisms, thus increasing the biogas yield. As the digestion temperature continues to increase, the higher temperature beyond optimum temperature would lower the activity of microorganisms, and make the anaerobic digestion process less efficient. Through the polynomial regression to fit the measured data in [9],[32],[36], the biogas production rate f_D can be modeled as follows,

$$f_{\mathrm{D}} = m(T_{\mathrm{Z}} - T_{\mathrm{O}})^2 + n \tag{1}$$

where T_{Z} and T_{O} are the actual digestion temperature and optimum temperature, respectively; m and n are the coefficients obtained from the data fitting. The optimum temperature T_{O} is 35°C for most of the mesophilic organisms [30]. In this study, a multi-energy thermal interaction model is formulated to investigate the digesting thermodynamic effects under external energy injections. Firstly, an R-C thermal network is modeled in Fig. 1 to capture temperature dynamics in the digester. The heat transfer and storage can be denoted by thermal resistance and capacitance [37]. The inside, wall and outside temperatures of the digester are represented by nodes with thermal potentials. The interior surfaces of digester walls are usually sprayed with insulation materials, such as sheet plastic and rubber, to offer thermal insulation against the cold [33]. Taking a digester with two-layer walls as an example, the internal wall node is linked with the digester inside node via two series resistors with resistances $R_{\mathrm{W1}}/2$ and R_{in}, while a peripheral wall node is connected with the outside node by two series resistances $R_{\mathrm{W2}}/2$ and R_{out}, as shown in Fig. 1. The thermal insulation of the two-layer walls are linked with two resistances $R_{\mathrm{W1}}/2$ and $R_{\mathrm{W2}}/2$. Then, the digesting thermal dynamics can be governed using the nodal analysis for thermal circuit, as follows,

$$C_{\mathrm{Z}} \frac{dT_{\mathrm{Z}}}{dk} = Q_{\mathrm{RES}} + \frac{T_{\mathrm{W1}} - T_{\mathrm{Z}}}{R_{\mathrm{in}} + R_{\mathrm{W1}}/2} \tag{2}$$

$$C_{\mathrm{W1}} \frac{dT_{\mathrm{W1}}}{dk} = \frac{T_{\mathrm{Z}} - T_{\mathrm{W1}}}{R_{\mathrm{in}} + R_{\mathrm{W1}}/2} + \frac{T_{\mathrm{W2}} - T_{\mathrm{W1}}}{R_{\mathrm{W2}}/2 + R_{\mathrm{W1}}/2} \tag{3}$$

$$C_{\mathrm{W2}} \frac{dT_{\mathrm{W2}}}{dk} = \frac{T_{\mathrm{out}} - T_{\mathrm{W2}}}{R_{\mathrm{out}} + R_{\mathrm{W2}}/2} + \frac{T_{\mathrm{W1}} - T_{\mathrm{W2}}}{R_{\mathrm{W1}}/2 + R_{\mathrm{W2}}/2} \tag{4}$$

$$Q_{\mathrm{RES}} = \eta_{\mathrm{B}} S_{\mathrm{ef}} + S_{\mathrm{hf}} \tag{5}$$

where R_{in}, R_{out}, R_{W1}, and R_{W2} are the thermal resistances for internal and external convective heat transfer, conductive heat transfer of the two-layer walls, respectively; Q_{RES} is the injected heating energy from RESs; T_{Z}, T_{out}, T_{W1}, and T_{W2} are the temperatures of digester inside and outside, the 1st and 2nd layer walls, respectively; C_{Z}, C_{W1}, and C_{W2} are thermal capacitances of digester inside, the 1st and 2nd layer walls, respectively; k denotes the scheduling time; η_{B} is the conversion efficiency of electric boiler; S_{ef} and S_{hf} denote the electricity and thermal energy feedback for digester heating, respectively. The thermal resistance and capacitance parameters of insulation materials adopted here were obtained from [32],[33],[37], and have validated against the historical data (e.g., digestion temperature, outside temperature, thermal energy for digester heating, etc.) for parameter tuning [36].

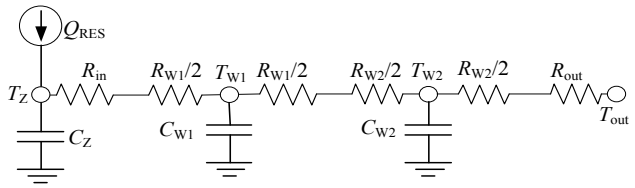

Fig. 1 R-C thermal network of digester inside and its surrounding walls

Here, (2), (3) and (4) indicate the thermal interactions for heat transfer among the external heating sources, digester inside, two-layer walls, and ambient environment in the closed digester. (5) represents the harvesting available renewable energy in the form of electricity and thermal energy for digester heating. Since the surrounding walls and ambient environment of digester at all directions are regarded as the same thermal resistances and capacitances, the thermodynamics are modeled by the thermal circuit in Fig.1 for digesting zone and digester wall on one direction. In order to decrease the computational efforts, a linearization method for generic nonlinear dynamic

models in [37] is adopted. The differential equations in (2)-(4) can be transformed into a state space form, and the system dynamics are linearized around a nearest equilibrium point to the system operating point. Then, the linearized state space realization model is discretized for numerical iterations, as follows,

$$x_{k+1} = Ax_k + Bu_k + Dd_k \tag{6}$$

$$y_k = Yx_k \tag{7}$$

where x_k is the state vector denoting the temperatures of nodes in thermal circuit at time k; y_k is the output vector denoting the temperature of digesting zone at time k; u_k represents the input vector of controllable electricity and thermal energy for digester heating at time k; d_k stores the uncontrollable inputs and system disturbances at time k, e.g., weather conditions and ambient temperature; A is the system state matrix and Y is the output matrix of the system; The B denotes the input matrix corresponding to the controllable variables and D stores the input matrix corresponding to the disturbance variables. In this study, Q_{RES} from external heating sources is the controllable input. It has been proved in [37],[38] that this linearization will not lead to significant truncation errors because of the small temperature range in the digester. Consequently, from the thermodynamics-based model in (1)-(7), the gain in biogas yield resulted from the biogas-solar-wind energy injections for heating digester can further be analyzed.

B. Biogas-Solar-Wind Energy Hub Framework

The multi-energy complementarities of hybrid biogas-solar-wind renewable portfolio can be fully exploited based on the digesting thermodynamic analysis. With the effects of digestion temperature on the biogas yield, the available thermal and electrical energy from solar and wind generation outputs are allowed to heat the digester, thereby facilitating the anaerobic digestion to increase biogas productions. The obtained biogas can be stored in a compressed gas storage tank to make it accessible for later use once there are inadequate wind and solar energy. The utilization of RESs for digester heating is a sustainable and effective way to overcome the low biogas production in cold climates, and also can enhance the penetration of volatile and intermittent RESs. Furthermore, the controllable CHP cogeneration of biogas plants can facilitate to offset the diurnal fluctuations of various RES outputs [12]. As an alternative to energy storage, the renewable electricity can be converted in the form of biogas and stored in the gas storage tank so as to alleviate the unnecessary discharging/charging of BES.

Fig. 2 illustrates a biogas-solar-wind hybrid renewable system with multi-energy carriers based on the concept of energy hub. The proposed energy hub framework is supplied by wind, solar and biomass energy which can be converted and conditioned through wind turbine (WT), photovoltaic thermal (PVT) system and digester into different energy carriers, e.g., electricity, heat and biogas. The PVT system is a renewable cogeneration system which combines thermal collectors and photovoltaic cells, and thus can produce low-temperature heat and electricity simultaneously from solar radiation [39]. In the energy hub, several energy conversion and storage devices, such as transformer, CHP, biogas furnace, BES, biogas storage tank, etc., are used to convert and control these energy carriers into desirable qualities and quantities to be consumed by electricity, heat/thermal, gas loads at the output port. The produced biogas is a versatile and flexible energy carrier, which can either directly supply the gas load, or be converted into electricity using the CHP gas engine. Waste heat from the engine as well as heat production from furnace and boiler can supply the thermal load or be used for digester heating. Both of BES and biogas tank can offer large storage capacities for available electricity and biogas. Hence, various converters and storages are integrated for combining and coupling these carriers to form redundant connections within the hub-internal energy, and can offer a certain degree of flexibility and synergies for multi-energy supplies.

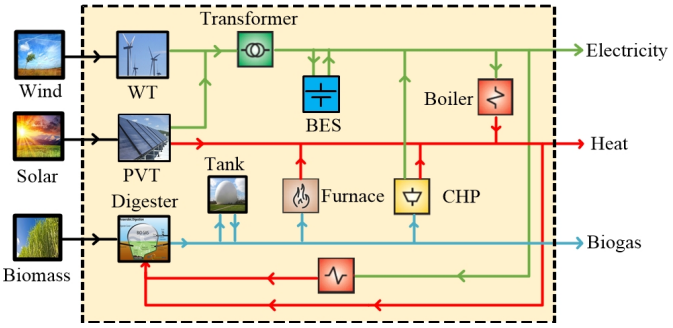

Fig. 2 Biogas-solar-wind integrated multi-energy supply framework

C. Steady-State Multi-Energy Coupling Matrix

In order to further analyze the inherent controllability and multi-energy couplings within the energy hub, a coupling matrix is formulated to model the conversion and storage of different energy carriers for the multi-input multi-output energy hub, as shown in (8). The elements of the matrix are coupling factors to represent the conversion efficiencies and hub-internal topology. For the single-input single-output converter device, such as electric boiler and furnace, the coupling factor expresses its steady-state energy efficiency. For multi-input and multi-output converter devices, since the input junctions of an energy carrier may connected to several converters, e.g., biogas is split up to the CHP and furnace, the dispatch factor is introduced in [18] to define the allocation of the total input to the devices converting this carrier, and the coupling factors should contain the products of dispatch factors and conversion efficiencies. In (8), W_{WT}, G_{PVT}, and E_{bio} are wind speed, solar irradiation, and biomass energy inputs, respectively; P_{BES} and V_{GS} are the net outputs of electricity and biogas for battery and biogas storage, respectively; The net power of BES, P_{BES}, is the subtraction of discharging power P_{dis} and charging power P_{ch}; L_e, L_h, and L_g are electricity, thermal, and gas loads; f_{WT} denotes the power conversion function of WT [4]; $f_{\mathrm{e,PVT}}$ and $f_{\mathrm{h,PVT}}$ are the output power and thermal functions of PVT in [39]; $\eta_{e,\mathrm{CHP}}$ and $\eta_{h,\mathrm{CHP}}$ are the gas-electric and gas-thermal efficiencies of CHP; η_{B} and η_{F} are conversion efficiencies of electric boiler and biogas furnace, respectively; Q_{bio} is the heat value of biogas; ν_{B}, ν_{CHP}, ν_{F}, ν_e, ν_h, and ν_g are the dispatch factors of input energy carriers to electric boiler, CHP, furnace, electricity, thermal, and biogas load, respectively.

The multi-carrier energy coupling model (8) is a highly nonlinear system due to the product of dispatch factors. Therefore, a state variable-based method in [23] is used to avoid the nonlinearity induced by dispatch factors. Here, the converter outputs and the direct connections are designated as state variables. Taking the electric boiler as an example, a state variable S_{B} is designated to represent its thermal output which is con-

nected with other state variables in Fig. 2. The input electricity consumption, which is determined by dispatch factor ν_{B} in (8), can be represented as $S_{\mathrm{B}}/\eta_{\mathrm{B}}$. As a result, the thermal output of electric boiler S_{B}, electricity output of CHP unit S_{CHP}, thermal output of biogas furnace S_{F}, electricity and thermal energy for digester heating S_{ef} and S_{hf}, are designated as state variables and combined with the input vector **E** in (8) to form a new state variable vector **E'** in (9). It can be found from (1)-(9) that the digesting temperature T_{Z} is an important state variable to determine the biogas production rate f_{D} in (1), and the electrical and thermal energy feedback to digester, S_{ef} and S_{hf}, can be used to maintain the optimum value of T_{Z}. With the sufficient biogas produced, the coordinated charging/discharging of biogas storage and BES for controllable variables, V_{GS} and P_{BES}, can offer great flexibility for multi-carrier energy scheduling in following different load demands in stand-alone Microgrids. Consequently, the coupling matrix **C** can further be reformulated to obtain an extended matrix **C'** in (9) to indicate the couplings between the state and output/input variables. Though the coupling matrix **C'** is nonlinear, it is sparser for efficient computational iterations, and also shows more flexible for the scalability with the integration of other energy sources. Based on the modelling of the proposed biogas-solar-wind energy hub and its coupling matrix in Section II, an optimal scheduling scheme for multi-carrier energy supplies will be further developed in Section III.

III. Multi-Carrier Energy Scheduling Scheme

A. Energy Scheduling Objective

Different energy carriers in the hub can be characterized by their cost and availability, and offer options for optimizing the system operating cost of multi-energy supplies [27]. The overall system scheduling cost should involve the costs incurred in the production, conversion, storage and consumption of multi-energy flows. As the proposed HRES is a 100% renewable energy system without energy production cost, the proposed cost-minimization scheduling scheme aims to control various hub-internal devices for optimal coordination among multi-carrier energy conversions, biogas and battery storages. For this multi-energy scheduling problem, the control variables include the battery charging and discharging power $P_{\mathrm{ch},k}$ and $P_{\mathrm{dis},k}$, biogas storage output $V_{\mathrm{GS},k}$, and state variables $S_{\mathrm{B},k}$, $S_{\mathrm{CHP},k}$, $S_{\mathrm{F},k}$, $S_{\mathrm{ef},k}$, and $S_{\mathrm{hf},k}$ for the kth time slot. The associated operating costs of energy hub in the scheduling process include the start-up/shut-down cost of CHP UC_k [40], energy loss costs due to energy conversions of various converters and storages LC_k, battery degradation cost caused by charging and discharging BC_k, and demand shedding cost DC_k, as follows,

$$UC_k = \mu_{\mathrm{CHP,SU}}\omega_k(1-\omega_{k-1}) + \mu_{\mathrm{CHP,SD}}\omega_{k-1}(1-\omega_k) \tag{10}$$

$$\begin{aligned} LC_k = \mu_{\mathrm{loss}}[&P_{\mathrm{ch},k}(1-\eta_{\mathrm{ch}}) + P_{\mathrm{dis},k}(1-1/\eta_{\mathrm{dis}}) + \\ &(S_{\mathrm{B},k}/\eta_{\mathrm{B}} + S_{\mathrm{ef},k})(1-\eta_{\mathrm{B}}) + S_{\mathrm{F},k}(1-\eta_{\mathrm{F}})/\eta_{\mathrm{F}} \\ &+ S_{\mathrm{CHP},k}(1-\eta_{e,\mathrm{CHP}}-\eta_{h,\mathrm{CHP}})/\eta_{e,\mathrm{CHP}}]\Delta k \end{aligned} \tag{11}$$

$$BC_k = \frac{(P_{\mathrm{ch},k}+P_{\mathrm{dis},k})\mu_{\mathrm{BES}}r_{\mathrm{BES}}\Delta k}{a_1[a_2(1-SOC_{\mathrm{BES},k})+a_3]\exp(a_4T_{\mathrm{out},k})E_{\mathrm{R}}(1-SOC_{\mathrm{BES,ref}})} \tag{12}$$

$$DC_k = \mu_{\mathrm{p}}(DL_{e,k} + DL_{h,k} + Q_{\mathrm{bio}}DL_{g,k})\Delta k \tag{13}$$

where $\mu_{\mathrm{CHP,SU}}$, $\mu_{\mathrm{CHP,SD}}$, μ_{loss}, and μ_{p} are the unit cost of CHP start-up, CHP shut-down, energy loss, and load shedding, respectively; ω_k is a binary variable, 1 or 0, to represent on or off state of CHP at the kth time slot; Δk is the length of per time slot; $DL_{e,k}$, $DL_{h,k}$ and $DL_{g,k}$ are the amount of load shedding for electricity, heat, gas at the kth time slot, respectively. The battery degradation cost model in [7] is adopted as the state of charge (SOC) and ambient temperature may cause considerable degradation to BES. μ_{BES} and r_{BES} are the capital cost and rated cycle life of batteries; $SOC_{\mathrm{BES,ref}}$ and $SOC_{\mathrm{BES},k}$ are the reference SOC and current SOC at the kth time slot, respectively; a_1, a_2, a_3 and a_4 are the coefficients of battery cycle life, and their values are taken from [7]; $\mathrm{E_R}$ is the total energy storage capacity of BES; η_{ch} and η_{dis} are the charging and discharging efficiency of batteries.

$$\underbrace{\begin{bmatrix} L_e \\ L_h \\ L_g \end{bmatrix}}_{\mathbf{L}} = \underbrace{\begin{bmatrix} f_{\mathrm{WT}}\nu_e & f_{e,\mathrm{PVT}}\nu_e & f_{\mathrm{D}}Q_{\mathrm{bio}}\nu_{\mathrm{CHP}}\eta_{e,\mathrm{CHP}}\nu_e & \nu_e & Q_{\mathrm{bio}}\nu_{\mathrm{CHP}}\eta_{e,\mathrm{CHP}}\nu_e \\ f_{\mathrm{WT}}\nu_{\mathrm{B}}\eta_{\mathrm{B}}\nu_h & (f_{e,\mathrm{PVT}}\nu_{\mathrm{B}}\eta_{\mathrm{B}} + f_{h,\mathrm{PVT}})\nu_h & f_{\mathrm{D}}Q_{\mathrm{bio}}(\nu_{\mathrm{CHP}}\eta_{e,\mathrm{CHP}}\nu_{\mathrm{B}}\eta_{\mathrm{B}} + \nu_{\mathrm{CHP}}\eta_{h,\mathrm{CHP}} + \nu_{\mathrm{F}}\eta_{\mathrm{F}})\nu_h & \nu_{\mathrm{B}}\eta_{\mathrm{B}}\nu_h & Q_{\mathrm{bio}}(\nu_{\mathrm{CHP}}\eta_{e,\mathrm{CHP}}\nu_{\mathrm{B}}\eta_{\mathrm{B}} + \nu_{\mathrm{CHP}}\eta_{h,\mathrm{CHP}} + \nu_{\mathrm{F}}\eta_{\mathrm{F}})\nu_h \\ 0 & 0 & f_{\mathrm{D}}\nu_{\mathrm{g}} & 0 & \nu_{\mathrm{g}} \end{bmatrix}}_{\mathbf{C}} \underbrace{\begin{bmatrix} W_{\mathrm{WT}} \\ G_{\mathrm{PVT}} \\ E_{\mathrm{bio}} \\ P_{\mathrm{BES}} \\ V_{\mathrm{GS}} \end{bmatrix}}_{\mathbf{E}} \tag{8}$$

$$\underbrace{\begin{bmatrix} L_e \\ L_h \\ L_g \end{bmatrix}}_{\mathbf{L}} = \underbrace{\begin{bmatrix} f_{\mathrm{WT}} & f_{e,\mathrm{PVT}} & 0 & 1 & 0 & -1/\eta_{\mathrm{B}} & 1 & 0 & -1 & 0 \\ 0 & f_{h,\mathrm{PVT}} & 0 & 0 & 0 & 1 & \eta_{h,\mathrm{CHP}}/\eta_{e,\mathrm{CHP}} & 1 & 0 & -1 \\ 0 & 0 & f_{\mathrm{D}} & 0 & 1 & 0 & -1/Q_{\mathrm{bio}}\eta_{e,\mathrm{CHP}} & -1/Q_{\mathrm{bio}}\eta_{\mathrm{F}} & 0 & 0 \end{bmatrix}}_{\mathbf{C'}} \underbrace{\begin{bmatrix} W_{\mathrm{WT}} \\ G_{\mathrm{PVT}} \\ E_{\mathrm{bio}} \\ P_{\mathrm{BES}} \\ V_{\mathrm{GS}} \\ S_{\mathrm{B}} \\ S_{\mathrm{CHP}} \\ S_{\mathrm{F}} \\ S_{\mathrm{ef}} \\ S_{\mathrm{hf}} \end{bmatrix}}_{\mathbf{E'}} \tag{9}$$

In order to enhance renewable energy utilization and system energy efficiency, an optimum multi-carrier energy scheduling scheme is developed to minimize the sum of the four operating costs in (10)-(13). The proposed scheduling scheme is formulated as a scenario-based stochastic optimization with rolling horizon strategy [41]. Each rolling decision step solves for the current time slot and looks ahead the remaining time slots considering the uncertainties of WT and PVT outputs as well as ambient temperature in future horizons. The scheduling objective function is to minimize the system operating cost of the current time slot k plus the expected operating cost of all scenarios from the next time slot $k+\Delta k$ to the end of the scheduling horizon, as follows,

$$\min \left\{ SC_k + \sum_{s=1}^{N_s} \rho_s \Big(\sum_{k=k+\Delta k}^{K_{\text{end}}} SC_{k,s} \Big) \right\} \tag{14}$$

$$SC_k = UC_k + LC_k + BC_k + DC_k \tag{15}$$

where SC_k and $SC_{k,s}$ are the system operating cost at current time slot k and the operating cost of scenario s at time slot k, respectively; K_{end} denotes the end of the scheduling horizon; N_{s} is the total number of scenarios for stochastic optimization; ρ_s is the probability of scenario s, and the sum of probabilities for all scenarios is equal to 1, e.g., $\sum_{s=1}^{Ns} \rho_s = 1$.

B. System Constraints

1) Multi-energy Balance Constraints: For a stand-alone Microgrid, load shedding is considered for multi-energy balance of supply and demand under extreme situations due to the volatility and intermittency of wind and solar energies. Hence, the amount of electricity, thermal, and gas load demand should be equal to the sum of the corresponding energy supply from energy hub and the amount of load shedding of interruptible load at each time slot respectively, as follows,

$$\begin{bmatrix} L_{e0,k} \\ L_{h0,k} \\ L_{g0,k} \end{bmatrix} = \begin{bmatrix} L_{e,k} \\ L_{h,k} \\ L_{g,k} \end{bmatrix} + \begin{bmatrix} DL_{e,k} \\ DL_{h,k} \\ DL_{g,k} \end{bmatrix} \tag{16}$$

where $L_{e0,k}$, $L_{h0,k}$, and $L_{g0,k}$ are the load demands for electricity, heat and gas at the kth time slot, respectively; $L_{e,k}$, $L_{h,k}$, and $L_{g,k}$ are the multi-carrier energy loads supplied and determined by coupling matrix (9).

2) Load Shedding Constraints: The amount of load shedding for each type of energy should be limited within its threshold,

$$\begin{aligned} DL_{e,k} &\le DL_{e,k,\max} \\ DL_{h,k} &\le DL_{h,k,\max} \\ DL_{g,k} &\le DL_{g,k,\max} \end{aligned} \tag{17}$$

where $DL_{e,k,\max}$, $DL_{h,k,\max}$, and $DL_{g,k,\max}$ denote the maximum limits of interruptible loads for electricity, heat, and gas at the kth time slot, respectively Here, $DL_{e,k}$, $DL_{h,k}$ and $DL_{g,k}$ are determined by the control variables in coupling matrix (9) and calculated using multi-energy balance equality constraints in (16).

3) Battery SOC Constraints: The SOC of BES should be limited to avoid the overcharging and overdischarging of batteries,

$$SOC_{\text{BES},k} = SOC_{\text{BES},k-\Delta k} + \frac{\eta_{\text{ch}} P_{\text{ch},k-\Delta k} \Delta k}{E_{\text{R}}} - \frac{P_{\text{dis},k-\Delta k} \Delta k}{\eta_{\text{dis}} E_{\text{R}}} \tag{18}$$

$$SOC_{\text{BES,min}} \le SOC_{\text{BES},k} \le SOC_{\text{BES,max}} \tag{19}$$

where $SOC_{\text{BES,min}}$ and $SOC_{\text{BES,max}}$ denote the lower and upper bounds of SOC of BES, respectively.

4) Battery Charging/Discharging Constraints: Since the fast charging/discharging rate would degrade the performance of batteries and thus shorten the lifespan [8], the charging/discharging power of BES should be limited as follows,

$$P_{\text{ch},k} \le P_{\text{ch,max}} \cdot \delta_k \tag{20}$$

$$P_{\text{dis},k} \le P_{\text{dis,max}} \cdot \varphi_k \tag{21}$$

$$\delta_k + \varphi_k \le 1 \tag{22}$$

where φ_k and δ_k are binary variables to represent the state of battery energy flow (charging or discharging) at the kth time slot; $P_{\text{ch,max}}$ and $P_{\text{dis,max}}$ are the allowable maximum charging and discharging power, respectively.

5) Digesting Temperature Constraints: The digestion temperature should be constrained to ensure the survival of anaerobic organisms, as follows,

$$T_{\text{Z,min}} \le T_{\text{Z},k} \le T_{\text{Z,max}} \tag{23}$$

where $T_{\text{Z,min}}$ and $T_{\text{Z,max}}$ are the lower and upper bounds of digestion temperature, respectively; In this paper, T_{Z} is an intermediate variable which can be solved through R-C thermodynamics-based network model in (2)-(7) and Fig.1.

6) Biogas Storage Constraints: The SOC and output of biogas storage tank should be constrained within their minimum and maximum bounds, as follows,

$$SOC_{\text{bio},k} = SOC_{\text{bio},k-\Delta k} - \frac{V_{\text{GS},k-\Delta k} \Delta k}{V_R} \tag{24}$$

$$SOC_{\text{bio,min}} \le SOC_{\text{bio},k} \le SOC_{\text{bio,max}} \tag{25}$$

$$V_{\text{GS,min}} \le V_{\text{GS},k} \le V_{\text{GS,max}} \tag{26}$$

where $SOC_{\text{bio},k}$ is the SOC of biogas storage at the kth time slot; V_{R} denotes the total volume of biogas storage; $SOC_{\text{bio,min}}$ and $SOC_{\text{bio,max}}$ are the lower and upper bounds of SOC of biogas storage, respectively; $\text{V}_{\text{GS},k}$ indicates the output of biogas discharging at the kth time when $\text{V}_{\text{GS},k} > 0$, and the biogas charging when $\text{V}_{\text{GS},k} < 0$; $\text{V}_{\text{GS,min}}$ and $\text{V}_{\text{GS,max}}$ are the lower and upper bounds of biogas storage output, respectively.

7) Boiler and Furnace Constraints: The outputs of electric boiler and furnace should be subject to their capacity limits as,

$$0 \le S_{\text{B},k} \le S_{\text{B,max}} \tag{27}$$

$$0 \le S_{\text{F},k} \le S_{\text{F,max}} \tag{28}$$

where $S_{\text{B,max}}$ and $S_{\text{F,max}}$ are the allowed maximum outputs of electric boiler and furnace, respectively.

8) CHP Unit Constraints: The electrical and thermal power outputs of CHP should be limited by its maximum and minimum capacities as well as the ramp rate [40], as follows,

$$\omega_k S_{\text{CHP,min}} \le S_{\text{CHP},k} \le \omega_k S_{\text{CHP,max}} \tag{29}$$

$$\omega_k H_{\text{CHP,min}} \le S_{\text{CHP},k} \eta_{h,\text{CHP}} / \eta_{e,\text{CHP}} \le \omega_k H_{\text{CHP,max}} \tag{30}$$

$$\left| S_{\text{CHP},k} - S_{\text{CHP},k-\Delta k} \right| \le P_{\text{CHP,ramp}} \tag{31}$$

where $S_{\text{CHP,min}}$ and $S_{\text{CHP,max}}$ are the lower and upper bounds of generation outputs of CHP unit, respectively; $H_{\text{CHP,min}}$ and $H_{\text{CHP,max}}$ denote the lower and upper bounds of CHP thermal outputs, respectively; $P_{\text{CHP,ramp}}$ is the ramp rate of CHP.

IV. Case Studies

A. System Data and Configuration

In this paper, a rural stand-alone Microgrid in Hunan, China, is presented to validate the performance of the proposed biogas-solar-wind renewable portfolio with the multi-energy supply scheme. In the rural areas, livestock and organic wastes are usually available plentiful, and can be used for fermentation to transform the wastes into biogas energy. In the rural Microgrid demonstration, a 600m^3 in-ground tubular digester was built as the reactor, and a 600m^3 biogas storage tank is also equipped. The installed capacities of PVT, WT, electric boilers, CHP unit, furnace, and BES are 150kW, 150kW, 200kW, 300kW, 200kW, and 400kWh, respectively. The seasonal variations of multi-energy demands and RES outputs are considered. The electrical, thermal and gas load profiles of two typical days in summer and winter seasons are shown in Fig. 3 and 4, respectively. It should be pointed out that the gas load represents the biogas consumption used for household cooking and lighting. The base loads of electricity, heat and gas are set to 350kW, 150kW, and 10m^3, respectively.

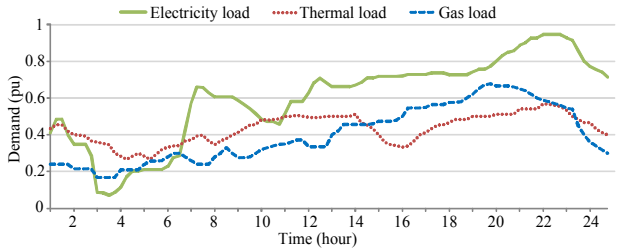

Fig. 3 Multi-energy load profiles of a typical day on summer season

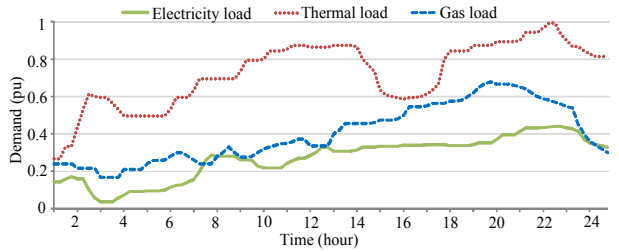

Fig. 4 Multi-energy load profiles of a typical day on winter season

The technical specifications of Microgrid components in the case study are summarized and listed in Table I. Besides, the load shedding limits, $DL_{e,k,\max}$, $DL_{h,k,\max}$, and $DL_{g,k,\max}$ are set to be 20% of each type of load at the kth time slot [22]. The rolling horizon optimization of the proposed energy hub scheduling scheme is performed for every 15 minutes over a 24-hour period. In each time slot, the forecasted RES outputs and ambient temperature can be procured from the historical data using nonlinear regression methods [4]. In order to capture the forecasting uncertainties, Monte Carlo simulations in [3] were implemented to obtain a set of scenarios in which each scenario expresses a possible status with renewable energy generation, and temperature prediction inaccuracies. These forecasting errors were assumed to follow a normal distribution function in [3], and then the scenario tree can be formed by several scenarios generated from historical forecasting data [42]. The corresponding scenario tree has 100 scenarios, and each scenario can be considered as a path with a possibility of 1/100. A scenario reduction technique in [28] is further utilized to reduce the computational cost, and thus only 10 scenarios are retained for the rolling optimization at each time slot.

TABLE I
Technical Specifications Of Microgrid Components In Hunan

Digester	$T_{Z,\min}$= 15°C	$T_{Z,\max}$= 55°C
	m = -0.125	n = 50
	Q_{bio}= 6.11 kWh/m^3	C_Z =749 kWh/°C
	C_{W1} =141.19 kWh/°C	C_{W2} =0.491 kWh/°C
	R_{in} =155.78×10^{-4} °C/kW	R_{out} =50.71×10^{-4} °C/kW
	R_{W1} =10.99×10^{-4} °C/kW	R_{W2} =85.78×10^{-4} °C/kW
Biogas storage	$V_{GS,\min}$= -200 m^3/h	$V_{GS,\max}$= 200 m^3/h
	$SOC_{\text{bio},\min}$= 0.1	$SOC_{\text{bio},\max}$= 1
Lead-acid BES	E_R = 400 kWh	η_{ch}= η_{dis}= 91.4%
	μ_{BES} = 24000 $	r_{BES} = 1000 cycles
	a_1= 3291	a_2= -4230
	a_3= 4332	a_4= -0.05922
	$SOC_{BES,\min}$= 0.1	$SOC_{BES,\max}$= 0.9
	$P_{ch,\max}$= 80 kW	$P_{dis,\max}$= 80 kW
CHP	$P_{CHP,ramp}$= 250 kW/h	
	$S_{CHP,\min}$= 5 kW	$S_{CHP,\max}$= 300 kW
	$\eta_{e,CHP}$= 0.4	$\eta_{h,CHP}$= 0.45
Boiler	$S_{B,\max}$= 200 kW	η_B= 0.75
Furnace	$S_{F,\max}$= 200 kW	η_F= 0.75
Unit cost	$\mu_{CHP,SU}$ = 8 $/start	$\mu_{CHP,SD}$ = 8 $/shut
	μ_{loss} = 1 $/kWh	μ_p = 10 $/kWh

B. Comparative Results and Analysis

For in-depth investigations on the effectiveness and superiority of the proposed methodology, three schemes are considered for comparative analysis and discussions: 1) Scheme 1 is the proposed coupled multi-energy scheduling scheme in Sections II and III; 2) Scheme 2 implements the energy hub scheduling without considering the battery degradation cost in (10); 3) Scheme 3 performs the energy supply model in the previous works [14],[35] in which the digester heating from RESs with digesting thermodynamic effects are not considered.

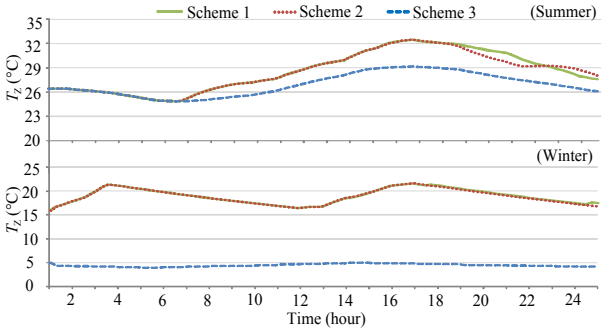

Fig. 5 The plot of daily digestion temperature curves with schemes 1-3

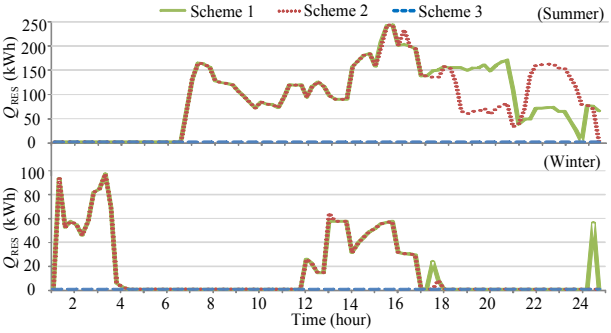

Fig. 6 The plot of daily heating energy injection with schemes 1-3

In this study, the proposed multi-carrier generation scheduling scheme is formulated as a scenario-based nonlinear and stochastic optimization model based on rolling horizon strategy. It is a mixed-integer nonlinear programming problem which can be implemented with the freely available YALMIP toolbox [43] in the MATLAB software and solved using the BONMIN solver on a personal computer with 4-GHz Intel Core i7 CPU and 8GB RAM. With the schemes 1-3, the curves of digestion temperature and the injected energy for digester heating are illustrated in Fig. 5 and Fig. 6, respectively. It can be found that, as there is abundant sunshine and wind during summertime, the outputs of PVT and WT are used to heat the digester for biogas yield enhancement, and thus the solar and wind energy can be harvested and stored in the biogas tank. In the winter season, the digestion temperature below 15°C in scheme 3 may cause biogas production to slow down or even stop as anaerobic organisms cannot survive in low-temperature environments. The proposed biogas-solar-wind complementarities in schemes 1 and 2 can tackle the detrimental impact from cold climates on biogas anaerobic organisms, and thereby facilitate the fast fermentation reaction rates for increasing the biogas yields.

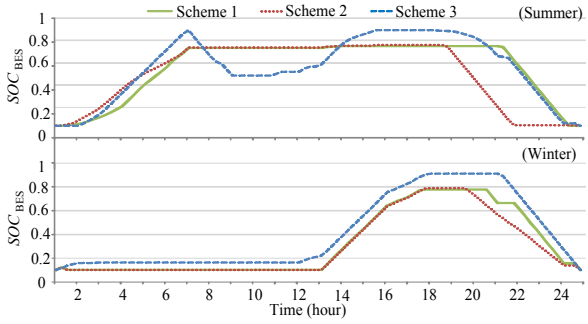

Fig. 7 The plot of daily battery SOC with schemes 1-3

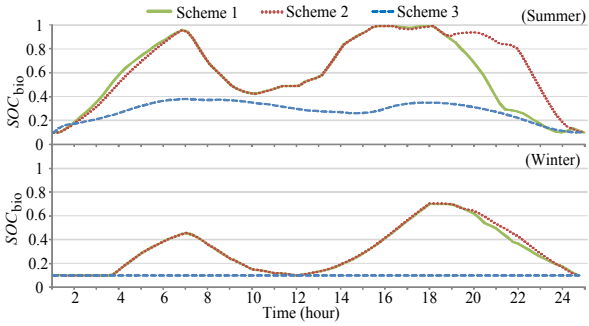

Fig. 8 The plot of SOC of biogas storage with schemes 1-3

Fig. 7-11 illustrate the output curves of BES, biogas storage, CHP, boiler and furnace with schemes 1-3. It can be found from Fig. 7-9 that compared with schemes 2 and 3, the proposed methodology can achieve a better coordination among various energy conversion, battery and biogas storage to enhance system energy efficiency. For example, during the hours 18-20 in the summer, the biogas storage and CHP in scheme 1 increase their outputs to satisfy the soaring loads while the BES remains unchanged. At hour 21, the output of CHP in scheme 1 decreases while the BES releases its power to follow the on-peak loads. However, in scheme 2, the CHP has to increase its output as BES has run out of its energy at hour 21. Besides, due to the energy loss and battery degradation cost from charging/discharging actions of BES, the biogas storage is prioritized as the reserve storage during hours 7-15 in the summer, as shown in Fig. 7-8. Furthermore, the multi-energy demands of residents in cold and hot seasons are quite different from each other, and the thermal load during the winter season is much higher than that in the summer season. Hence, it can be observed from Fig. 9-11 that most of the thermal load is supplied by CHP unit in the summer, and the thermal load in the winter is jointly supplied by CHP, boiler, and furnace.

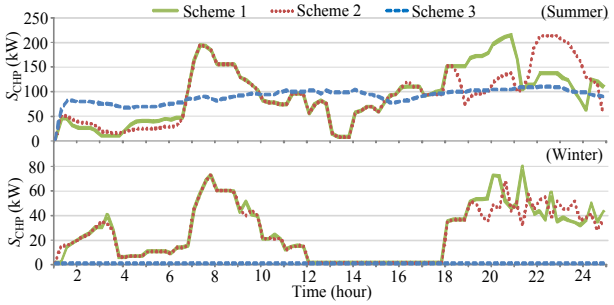

Fig. 9 The plot of daily power outputs of CHP with schemes 1-3

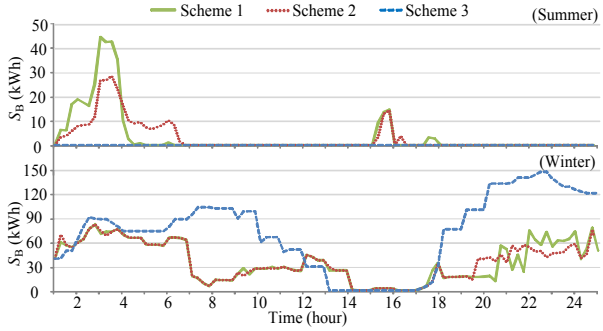

Fig. 10 The plot of daily energy outputs of boiler with schemes 1-3

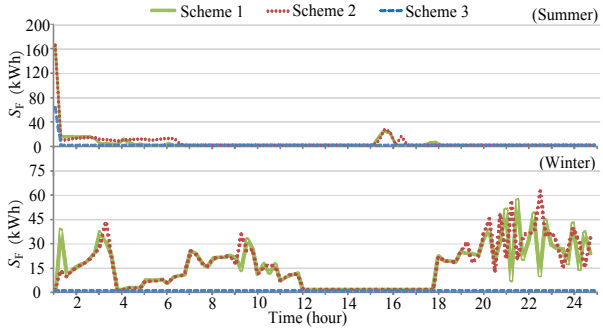

Fig. 11 The plot of daily energy outputs of furnace with schemes 1-3

The previous field investigations in Hunan indicate that a major difficulty is associated with biogas energy utilization due to the lack of solar radiation during the winter season. In order to demonstrate the performance of the proposed scheduling scheme under extreme weather conditions, Fig. 12 illustrates the curves of digestion temperature and CHP output on a winter day without solar energy. It can be found that, without the heating energy from PVT, the digestion temperature as well as biogas yield decrease significantly. Moreover, with the schemes 1-3, the curves of digestion temperature and CHP output on a winter day without solar and wind energy are plotted in Fig. 13. Since the digester heating from RESs is not considered, scheme 3 cannot provide sufficient biogas yield for energy supply in winter season. Therefore, it is concluded from Fig. 12 and 13 that the digesting thermodynamic effect is effective to maintain the biogas production for ensuring the multi-energy supplies under extreme weather conditions.

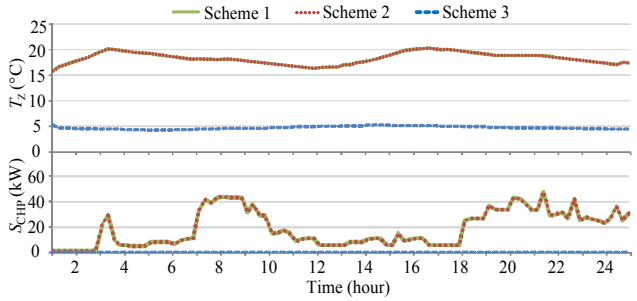

Fig. 12 The plot of scheduling results on a winter day with no solar

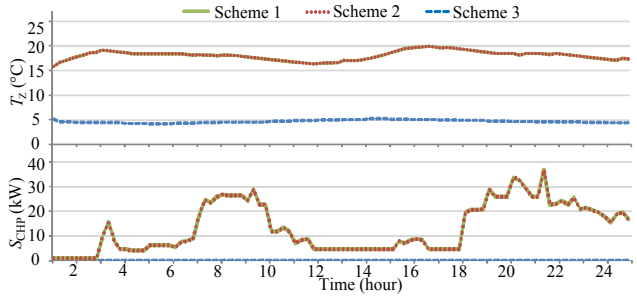

Fig. 13 The plot of scheduling results on a winter day with no solar and wind

TABLE II
COMPARATIVE PERFORMANCE RESULTS ON SUMMER SEASON OF SCHEMES 1-3

Scheme	1	2	3
System operating cost ($)	**1040.96**	1044.47	4386.37
Biogas yield (m^3)	**4226.42**	4221.77	3991.30
Battery degradation cost ($)	**68.42**	76.88	98.24
Energy loss (kWh)	964.55	959.59	**913.29**
Load shedding (kWh)	**0**	0	336.68
Solar-wind accommodation (%)	**100**	100	66.70

TABLE III
COMPARATIVE PERFORMANCE RESULTS ON WINTER SEASON OF SCHEMES 1-3

Scheme	1	2	3
System operating cost ($)	**774.17**	776.94	24412.63
Biogas yield (m^3)	**1691.47**	1685.10	0
Battery degradation cost ($)	**22.18**	28.78	23.82
Energy loss (kWh)	727.99	**724.16**	1299.01
Load shedding (kWh)	**0**	0	2308.98
Solar-wind accommodation (%)	**100**	100	90.2

TABLE IV
COMPARATIVE PERFORMANCE RESULTS WITHOUT SOLAR OF SCHEMES 1-3

Scheme	1	2	3
System operating cost ($)	**18484.24**	18484.24	43928.48
Biogas yield (m^3)	**1537.90**	1537.90	0
Battery degradation cost ($)	**0**	0	20.66
Energy loss (kWh)	**902.74**	902.74	1013.82
Load shedding (kWh)	**1737.45**	1737.45	4289.40
Solar-wind accommodation (%)	**100**	100	100

Table II-IV gives the 24-hour scheduling results on the typical days on summer and winter as well as a winter day without solar. The system performance results on operating cost, biogas yield, battery degradation cost, energy loss, load shedding, and solar-wind accommodation obtained with schemes 1-3 are further compared. Since the degradation cost is considered in scheme 1, the charging/discharging actions of BES in scheme 1 are less frequent and more economical than that of scheme 2, and thus give rise to lower operation cost in Table II-IV. On the other hand, it can be found from Table II and III that the energy loss costs account for a large proportion of the system operating cost. Due to the seasonal variations on multi-energy demands and RES generations, the total amount of multi-energy load in the summer is larger than that in the winter for the studied Microgrid, and the biogas production would also significantly increase because of high ambient temperature in the summer. It is clear from Fig. 9 that the outputs of CHP unit in the summer are much larger than those in the winter, and causes much more energy loss from the multi-energy conversion processes. Thus, the energy loss costs in the summer day are much higher than those in the winter day, which gives rise to considerably large system operating cost in Table II.

It is also observed that the proposed methodology can provide flexible multi-energy utilization to accommodate solar-wind energy variability with the least amount of load shedding. As BES has relatively higher charging/discharging efficiency, the deep charging/discharging in scheme 2 leads to the less energy loss and higher degradation cost in Table III. All in all, the comparative results can demonstrate the superior performance of the proposed scheme 1 on efficient energy management and conversion, especially on the improvements on operating cost and renewable energy penetration.

C. *Influence of BES Capacity*

In order to analyze the effects of BES capacity on the system performance, the proposed scheme is performed under different battery capacities varying from 0.5 per unit to 1.5 per unit with the base capacity 400kWh. Fig. 14 illustrates the performance results of demand shedding cost, solar-wind accommodation, battery degradation cost and system operation cost considering different BES capacities.

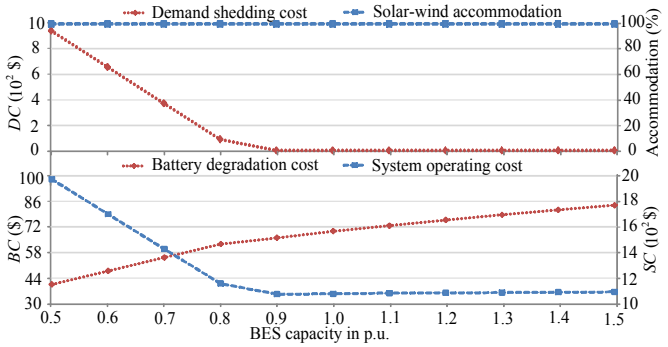

Fig. 14 system performance results versus different battery rating

With the increase of BES capacity from 0.5 to 0.9 per unit, the battery degradation cost *BC* gradually increases while system operation cost *SC* gradually decreases. It is clear that the load shedding occurs at low-capacity battery and decreases to 0 at 0.9 per unit. With the proposed biogas-solar-wind complementarities, abundant solar and wind energy can be harvested in the form of biogas, and thus the solar-wind accommodation stays at 100% under different BES capacities. Therefore, it can then be concluded that the proposed methodology can lower the dependence on battery storages, and perform well with lower battery capacity. The results also confirm that the utilization of wind and solar energy for digester heating can provide a feasible solution to address the integration challenge of high penetration of variable and intermittent RESs.

V. Conclusion

In this paper, the biogas-solar-wind energy complementarities are proposed to form a 100% renewable energy hub framework for stand-alone Microgrids, and an optimal multi-energy scheduling scheme is developed for coordination of production, conversion, storage, and consumption of electricity, heat, and gas. The greatly improvements of the proposed methodology are due to the utilizations of biogas thermodynamic effects for flexible multi-energy conversion and storage. It has been found from simulation studies that, with the coupling interaction and energy storage among biogas and other RESs, the overcharging and deep discharging of BES can be avoided to prolong the lifetime of batteries. Comparative results demonstrate the superiority of the proposed method to enhance renewable penetration and biogas yield with a significant reduction in operation costs, and also exhibit great potential to provide diversified energy supplies for residents in off-grid remote.

References

[1] M. H. Nehrir, C. Wang, K. Strunz, *et al*., "A review of hybrid renewable/alternative energy systems for electric power generation: Configurations, control, and applications," *IEEE Trans. Sustain. Energy*, vol. 2, no. 4, pp. 392-403, Oct. 2011.

[2] T. A. Nguyen and M. L. Crow, "Stochastic optimization of renewable-based Microgrid operation incorporating battery operating cost," *IEEE Trans. Power Syst*., vol. 31, no. 3, pp. 2289-2296, May 2015.

[3] W. Su, J. Wang, and J. Roh, "Stochastic energy scheduling in Microgrid with intermittent renewable energy resources," *IEEE Trans. Smart Grid*, vol. 5, no. 4, pp. 1876-1883, Jul. 2014.

[4] A. Arabali, M. Ghofrani, and M. Etezadi-Amoli, *et al*., "Stochastic performance assessment and sizing for a hybrid power system of solar/wind/energy storage," *IEEE Trans. Sustain. Energy*, vol. 5, no. 2, pp. 363-371, Apr. 2014.

[5] C. O'Dwyer, L. Ryan, and D. Flynn, "Efficient large-scale energy storage dispatch: Challenges in future high renewables systems," *IEEE Trans. Power Syst*., vol. 32, no. 5, pp. 3439-3450, Sep. 2017.

[6] L. Feng, J. Zhang, G. Li, *et al*., "Cost reduction of a hybrid energy storage system considering correlation between wind and PV power," *Protection and Control of Modern Power Systems*, pp.1-9, Dec. 2016, DOI: 10.1186/s41601-016-0021-1.

[7] B. Zhou, X. Liu, and Y. Cao, *et al*., "Optimal scheduling of virtual power plant with battery degradation cost," *IET Gen., Trans. Distrib*., vol. 10, no. 3, pp. 712-725, Feb. 2016.

[8] I. Duggal and B. Venkatesh, "Short-term scheduling of thermal generators and battery storage with depth of discharge-based cost model," *IEEE Trans. Power Syst*., vol. 30, no. 4, pp. 2110-2118, Jul. 2015.

[9] C. Mao, Y. Feng, and X. Wang, *et al*., "Review on research achievements of biogas from anaerobic digestion," *Renew. Sustain. Energy Rev.*, vol. 45, pp. 540-555, May 2015.

[10] H. Hahn, W. Ganagin, and K. Hartmann, *et al*., "Cost analysis of concepts for a demand oriented biogas supply for flexible power generation," *Bioresource technology*, vol. 170, pp. 211-220, Oct. 2014.

[11] M. Prakash, A. Sarkar, and J. Sarkar, *et al*., "Proposal and design of a new biomass based syngas production system integrated with combined heat and power generation," *Energy*, vol. 133, no. 15, pp. 986-997, Aug. 2017.

[12] P. A. Ostergaard, "Comparing electricity, heat and biogas storages' impacts on renewable energy integration," *Energy*, vol. 37, no. 1, pp. 255-262, Jan. 2012.

[13] H. Hahn, B. Krautkremer, and K. Hartmann, *et al*., "Review of concepts for a demand-driven biogas supply for flexible power generation," *Renew. Sustain. Energy Rev.*, vol. 29, pp. 383-393, Jan. 2014.

[14] S. G. Sigarchian, R. Paleta, and A. Malmquist, *et al*., "Feasibility study of using a biogas engine as backup in a decentralized hybrid (PV/wind/battery) power generation system–Case study Kenya," *Energy*, vol. 90, pp. 1830-1841, Oct. 2015.

[15] M. Mudasser, E. K. Yiridoe, and K. Corscadden, "Cost-benefit analysis of grid-connected wind–biogas hybrid energy production, by turbine capacity and site," *Renew. Energy*, vol. 80, pp. 573-582, Aug. 2015.

[16] Md. M. Rahman, M. M. Hasan, and J. V. Paatero, *et al*., "Hybrid application of biogas and solar resources to fulfill household energy needs: A potentially viable option in rural areas of developing countries," *Renew. Energy*, vol. 68, pp. 35-45, Aug. 2014.

[17] M. Geidl, G. Koeppel, and P. Favre-Perrod, *et al*., "Energy hubs for the future," *IEEE Power Energy Mag.*, vol. 5, no. 1, pp. 24-30, Jan.-Feb. 2007.

[18] M. Geidl and G. Andersson, "Optimal power flow of multiple energy carriers," *IEEE Trans. Power Syst*., vol. 22, no. 1, pp. 145-155, Feb. 2007.

[19] M. Geidl, "Integrated modeling and optimization of multi-carrier energy systems," Ph.D. dissertation, Swiss Fed. Inst. Technol., ETH, Zurich, Switzerland, 2007.

[20] T. Krause, G. Andersson, K. Frohlich, and A. Vaccaro, "Multiple-energy carriers: modeling of production, delivery, and consumption," *Proc. IEEE*, vol. 99, no. 1, pp. 15-27, Jan. 2011.

[21] M. Moeini-Aghtaie, A. Abbaspour, and M. Fotuhi-Firuzabad, *et al*., "A decomposed solution to multiple-energy carriers optimal power flow," *IEEE Trans. Power Syst*., vol. 29, no. 2, pp. 707-716, Mar. 2014.

[22] X. Zhang. M. Shahidehpour, A. Alabdulwahab, and A. Abusorrah, "Optimal expansion planning of energy hub with multiple energy infrastructures," *IEEE Trans. Smart Grid*, vol. 6, no. 5, pp. 2302-2311, Sep. 2015.

[23] C. Shao, X. Wang, and M. Shahidehpour, *et al*., "An MILP-based optimal power flow in multicarrier energy systems," *IEEE Trans. Sustain. Energy*, vol. 8, no. 1, pp. 239-248, Jan. 2017.

[24] Y. Wang, N. Zhang, and C. Kang, *et al*., "Standardized matrix modeling of multiple energy systems," *IEEE Trans. Smart Grid*, DOI: 10.1109/TSG.2017.2737662, 2017.

[25] P. Mitchell and S. Skarvelis-Kazakos, "Control of a biogas co-firing CHP as an energy hub", in *Proc. Int. Universities Power Eng. Conf*., 2015, pp. 1-6.

[26] S. Chen, Z. Wei, and G. Sun, *et al*., "Multi-linear probabilistic energy flow analysis of integrated electrical and natural-gas systems," *IEEE Trans. Power Syst*., vol. 32, no. 3, pp. 1970-1979, May 2017.

[27] M. Rastegar, M. Fotuhi-Firuzabad, H. Zareipour, *et al*., "A probabilistic energy management scheme for renewable-based residential energy hubs," *IEEE Trans. Smart Grid*, vol. 8, no. 5, pp. 2217-2227, Sep. 2017.

[28] A. Dolatabadi, B. Mohammadi-ivatloo, M. Abapour, and S. Tohidi, "Optimal stochastic design of wind integrated energy hub," *IEEE Trans. Ind. Informat*., vol. 13, no. 5, pp. 2379-2388, Oct. 2017.

[29] G. Taljan, C. Cañizares, and M. Fowler, *et al*., "The feasibility of hydrogen storage for mixed wind-nuclear power plants," *IEEE Trans. Power Syst*., vol. 23, no. 3, pp. 1507-1518, Aug. 2008.

[30] K. Orehounig, R. Evins, and V. Dorer, "Integration of decentralized energy systems in neighbourhoods using the energy hub approach," *Applied Energy*, vol. 154, no. 15, pp. 277-289, Sep. 2015.

[31] M. Mohammadi, Y. Noorollahi, and B. Mohammadi-ivatloo, *et al*., "Energy hub: From a model to a concept. A review," *Renew. Sustain. Energy Rev.*, vol. 80, pp. 1512-1527, Dec. 2017.

[32] R. Feng, J. Li, and T. Dong, "Performance of a novel household solar heating thermostatic biogas system," *Appl. Thermal Eng.*, vol. 96, pp. 519-526, Mar. 2016.

[33] V. C. Weatherford and Z. J. Zhai, "Affordable solar-assisted biogas digesters for cold climates: Experiment, model, verification and analysis," *Applied Energy*, vol. 146, no. 15, pp. 209-216, May 2015.

[34] C. Lai and M. McCulloch, "Sizing of stand-alone solar PV and storage system with anaerobic digestion biogas power plants," *IEEE Trans. Ind. Electronics*, vol. 64, no. 3, pp. 2112-2121, Mar. 2017.

[35] M. Hohmann, C. Waibel, R. Evins, and J. Carmeliet, "Multi-objective optimization of the design and operation of an energy hub for the EMPA campus", in *Proc. Int. Conf. Cleantech Smart Cities Buildings*, 2015, pp. 1-6.

[36] X. Pu, L. Deng, and Y. Yin, *et al.* "Economic benefit analysis on large and middle-scale biogas plants with different heating methods," *Transactions of the CSAE*, vol. 26, no. 7, pp. 281-284, July 2010. (in Chinese)

[37] M. Maasoumy, Controlling energy-efficient buildings in the context of smart grid: a cyber physical system approach Univ. California, Elect. Eng. Dept., Berkeley, 2013, Tech. Rep. UCB/EECS-2013-244.

[38] W. J. Mai and C. Y. Chung, "Economic MPC of aggregating commercial buildings for providing flexible power reserve," *IEEE Trans. Power Syst*., vol. 30, no. 5, pp. 2685-2694, Sep. 2015.

[39] S. Thakare, K. Priya, C. Ghosh, and S. Bandyopadhyay, "Optimization of photovoltaic-thermal based cogeneration system through water replenishment profile," *Solar Energy*, vol. 133, pp. 512-523, Aug. 2016.

[40] A. Anvari-Moghaddam, H. Monsef, and A. Rahimi-Kian, "Optimal smart home energy management considering energy saving and a comfortable lifestyle," *IEEE Trans. Smart Grid*, vol. 6, no. 1, pp. 324-332, Jan. 2015.

[41] R. Palma-Behnke, C. Benavides, and F. Lanas, *et al*., "A Microgrid energy management system based on the rolling horizon strategy," *IEEE Trans. Smart Grid*, vol. 4, no. 2, pp. 996-1006, June 2013.
[42] Climate data, 2016. [Online]. Available: http://data.cma.cn/en/?r=data/index&cid=6d1b5efbdcbf9a58.
[43] J. Löfberg, "YALMIP: A toolbox for modeling and optimization in MATLAB," in *Proc. CACSD Conf*., 2004, pp. 284-289.

Bin Zhou (S'11-M'13-SM'17) received the B.Sc. degree in electrical engineering from Zhengzhou University, Zhengzhou, China, in 2006, the M.S. degree in electrical engineering from South China University of Technology, Guangzhou, China, in 2009, and the Ph.D. degree from The Hong Kong Polytechnic University, Hong Kong, in 2013. Afterwards, he worked as a Research Associate and subsequently a Postdoctoral Fellow in the Department of Electrical Engineering of The Hong Kong Polytechnic University. Now, he is an Associate Professor in the College of Electrical and Information Engineering, Hunan University, Changsha, China. His main fields of research include smart grid operation and planning, renewable energy generation, and energy efficiency.

Da Xu received the B.Sc. degree in automation from Wuhan University of Technology, Wuhan, China, in 2015. He is currently pursuing the Ph.D. degree at the College of Electrical and Information Engineering in Hunan University, Changsha, China. His major research interests include smart grid operation and optimization, renewable energy generation.

Canbing Li (M'06-SM'13) received the B.Sc. degree and the Ph.D. degree both in electrical engineering from Tsinghua University, Beijing, China, in 2001 and 2006, respectively. He is currently a Professor with the College of Electrical and Information Engineering, Hunan University, Changsha, China. His research interests include smart grid, energy efficiency and energy policy.

Chi Yung Chung (M'01–SM'07–F'16) received the B.Eng. degree (with First Class Honors) and the Ph.D. degree in electrical engineering from The Hong Kong Polytechnic University, Hong Kong, in 1995 and 1999, respectively. He worked in Powertech Labs, Inc., Surrey, BC, Canada, the University of Alberta, Edmonton, AB, Canada, and The Hong Kong Polytechnic University, China. He is currently a Professor and the SaskPower Chair in Power Systems Engineering in the Department of Electrical and Computer Engineering at the University of Saskatchewan, Saskatoon, SK, Canada. His research interests include power system stability, control, planning and operation, computational intelligence applications, and electric vehicle charging.

Yijia Cao (M'98-SM'13) received the B.Sc. degree in electrical engineering from Xi'an Jiaotong University, Xi'an, China, in 1988, and the Ph.D. degree from Huazhong University of Science and Technology, Wuhan, China, in 1994. He is currently a Chair Professor and Vice President in the College of Electrical and Information Engineering, Hunan University, Changsha, China. His research interests include power system cascading failure, smart grid information technology, smart grid operation and optimization.

Ka Wing Chan (M'98) received the B.Sc. (with First Class Honors) and Ph.D. degrees in electronic and electrical engineering from the University of Bath, Bath, U.K., in 1988 and 1992, respectively. He currently is an Associate Head and Associate Professor in the Department of Electrical Engineering of The Hong Kong Polytechnic University. His general research interests include smart grid and renewable energy, power system stability analysis and control, power system planning and optimization, real-time power system simulation.

Qiuwei Wu (M'08-SM'15) received the B.Eng. and M.Eng. degrees from Nanjing University of Science and Technology, Nanjing, China, in 2000 and 2003, respectively, both in power system and automation, and the Ph.D. degree in power system engineering from Nanyang Technological University, Singapore, in 2009. He worked as a senior R&D engineer in Vestas Technology R&D Singapore Pte. Ltd. from March 2008 to October 2009. Now, he is an Associate Professor in the Centre for Electric Power & Energy, Department of Electrical Engineering, Technical University of Denmark (DTU). His research interests include smart grids, wind power, and active distribution networks.